Crystallization Rates of Matched Fractions of $MgCl_2$-Supported Ziegler Natta and Metallocene Isotactic Poly(Propylene)s. 1. The Role of Chain Microstructure†

Rufina G. Alamo* and Jose A. Blanco

Department of Chemical Engineering, Florida Agricultural and Mechanical University and Florida State University, Tallahassee, Florida 32310-6046

Pawan K. Agarwal

Exxon-Mobil Co., Baytown Polymers Center, Baytown, Texas 77522-5200

James C. Randall

2710 Ridge Road, Steamboat Springs, Colorado 80487

Received October 3, 2002; Revised Manuscript Received December 24, 2002

ABSTRACT: The microstructures of two poly(propylene)s with matched molar masses and overall defect concentrations are inferred from the crystallization behavior of their narrow molar mass fractions. One poly(propylene) was produced with a $MgCl_2$-supported Ziegler−Natta catalyst and the other with a metallocene catalyst. The fractions obtained from the metallocene isotactic poly(propylene) display a range in molar masses but each has the same defect concentration indicating a uniform intermolecular concentration of defects in the parent metallocene isotactic poly(propylene). These fractions provide direct evidence of the "single site" character of the metallocene catalyst. The variations of crystallization rates with molar mass reflect different chain diffusion/transport phenomena that are governed by the remnant entanglement state of the melt during crystallization. The molar mass fractions obtained from the ZN-iPP confirm that the interchain distribution of the nonisotactic content is broad in this polymer. The stereodefects are more concentrated in the low molar mass fractions. Furthermore, the invariance of the linear growth rates among the ZN fractions and the lack of formation of any significant content of the γ polymorph, even in the most defected fraction, is consistent with a nonrandom, blocky intramolecular distribution of defects in the ZN-iPP molecules. In contrast to the growth rates, the overall crystallization rates are a direct function of the primary nucleation density, which varies among the fractions and the unfractionated iPPs. Hence, the measured overall crystallization rates would be correlated with nucleation density and not necessarily with the microstructure of the iPP molecules. The crystallization data are also interpreted in light of results from pentad/heptad distributions predicted by two-state and three-state statistical models. Parameters from the models allow the prediction of sequence distribution curves that could be used to evaluate each of the models as to their consistency with the crystallization rate data.

Introduction

Isotactic poly(propylene)s prepared with "classical" heterogeneous Ziegler−Natta catalyst systems (ZN-iPP) are complex because a distribution of various types of catalyst sites leads to a mixture of poly(propylene) molecules having strongly differing intermolecular stereosequence distributions. In contrast, poly(propylene)s prepared with the single-sited metallocene family of isotactic poly(propylene) catalysts (M-iPP) should have uniform intermolecular stereosequence distributions.[1,2] The identification of types, concentrations and distributions of stereosequences found in various poly(propylene)s is customarily carried out by ^{13}C NMR. Such structural information is important, not only as a way to correlate with the physical properties of these materials but also as a means to extract information concerning the nature of the catalyst sites and the mechanisms of the polymerization processes.

The influence of catalyst type on the microstructure of various ZN-iPPs has often been reevaluated as higher field NMR spectrometers with higher resolution and sensitivity became available.[3−10] In most of these previous studies, ^{13}C NMR analyses of structural defects have relied upon analyses of either whole polymers,[2−4] poly(propylene)s where an atactic poly(propylene) component had been removed after crystallization from xylene[5−9] or fractions from a parent ZN-iPP.[11−14] Some level of fractionation is required in the microstructural analyses of ZN-iPP to ensure that the NMR characterization is performed on crystalline chains only without interfering contributions from atactic components. It was shown that valuable structural information can be obtained by studying different fractions from a parent poly(propylene) and analyzing the stereosequence distribution of each of the fractions utilizing ^{13}C NMR.[11−14]

The crystallization behaviors of ZN-iPPs and M-iPPs have been reported in separate publications[15−21] but a direct comparison of the physical properties and crystallization behavior of these two types of poly(propylene)s, matched by molar mass and defect concentrations, has yet to be presented. It is the objective of this work to fractionate such a matched pair of ZN-iPP and M-iPP and to compare the structural and crystallization characteristics of the individual fractions with that observed for the whole, parent polymers. This type of study is needed to document the nature of inter- and intramo-

* Corresponding author. E-mail: alamo@eng.fsu.edu.

† Dedicated to Prof. L. Mandelkern on the occasion of his 80th birthday.

10.1021/ma021549g CCC: $25.00
Published on Web 02/14/2003

lecular microstructures that leads to differences in crystallization properties. A highly isotactic M-iPP and a corresponding ZN-iPP of the industrial type were selected. From this study, it is possible to determine in detail how poly(propylene) microstructures, differing at inter- and intramolecular levels, can affect the crystallization behavior of isotactic poly(propylene)s.

The influence of the type of catalyst and polymerization process on microstructures of industrial ZN poly(propylene)s has been studied by different investigators.[11−14,22−23] TREF [14,22] and solvent gradient extraction[11−13] led to fractions of increasing isotacticity and increasing molar mass, a result that clearly indicated a nonuniform interchain composition of defects. They also observed that most of the fractions contained syndiotactic *rrrr* pentads and, as in other works,[7−13,24−26] it was proposed that some of the propagation errors were "blocky" in nature. Thus, the presence of stereoblocks in the ZN-iPP was inferred or suspected by most previous investigators and emphasized in Busico et al.'s latest work.[25]

Since it is important to identify the possibility of a nonrandom intramolecular distribution or blocky stereosequences in iPP chains, other types of physical evidence must be utilized in conjunction with ^{13}C NMR. This is the only approach that will satisfy the ultimate goal of correlating molecular microstructures with physical properties. For this purpose, indirect methods must be used to identify the intramolecular microstructure of the iPP molecule. One example is a recent publication in which a proposed blocky microstructure of highly defective iPPs was deduced by their crystallization properties.[27]

Different stereodefect distributions have been associated with quite different crystallization rates, even within a blocky microstructure. For example, in the crystallization process, short, isolated randomly distributed defected blocks will act as any other noncrystallizable single defect, retarding the crystallization rate and reducing the crystallinity and the melting temperature of the defected chain with respect to a defect free iPP chain. Moreover, noncrystallizable long defective blocks will have little or no effect upon the crystallization properties of long isotactic blocks of the chain. In the present work, we document the nature of the intermolecular defect distribution from GPC and NMR analyses of molecular fractions of ZN and metallocene types iPPs. Furthermore, indirect analyses are used to extract the intramolecular microstructure of the ZN poly(propylene)s. Focus is given to the analysis of the crystallization rates as a parameter that is a function of the defect microstructure.

Previous stereochemical analyses of the sequences of ZN fractions obtained by successive extractions with *n*-alkanes solvents were interpreted on the basis of two or three state models developed by Chûjö,[28] Doi,[29] and Busico et al.[25] to simulate a mixture of poly(propylene) chains produced by multisited Ziegler−Natta catalysts.[4,5,30] It is important to examine both the average microstructures and microstructural distributions of Ziegler−Natta poly(propylenes) in light of their crystallization behavior. Therefore, in a separate part of this work,[31] ^{13}C NMR data will be analyzed utilizing all of the current as well as some newly modified two state and three state statistical models. Each model was evaluated on how closely the predicted microstructural distributions conformed to the observed rates of crystallization.[31] The various models were also evaluated on the consistency of microstructural changes from fraction to fraction for the ZN-iPP where, from fractionation data, the average stereodefect level was observed to decrease with increasing molar mass. The results of a slight modification to the Busico three-state model,[25] utilizing first order Markovian statistics for the symmetric chain component instead of Bernoullian statistics, are discussed in the present paper. These results were found to be consistent with both the linear growth rates and fractionation data in addition to predicting the observed ^{13}C NMR pentad/heptad distributions and average sequence lengths.

The possibility of a nonrandom distribution of defects in the ZN-iPP will be discussed in the present paper from an analysis of the crystallization rates of the various molecular fractions. In addition, the crystallization rates of molecular fractions obtained from a M-iPP, will be compared to those from a ZN-iPP with a similar overall defect content. The value of comparisons with the M-iPP lies in the fact that we found the latter to have a random and uniform intra- and intermolecular distributions of stereodefects.

Experimental Section

Materials. The unfractionated poly(propylene)s were supplied by ExxonMobil. The ZN-iPP was obtained with one of the latest $MgCl_2$-supported industrial catalysts, and the metallocene iPP was obtained with an Exxpol Kaminsky type of catalyst.[32] The molecular characterization data, as per molar mass, molar mass distribution, and percentage of stereo- and regiodefects, are listed in Table 1. Only stereodefects were found in the ZN-iPP sample while both stereo- and 2,1-*erythro*-regiodefects were found in the metallocene iPP. These poly(propylene)s were chosen because they both comprise the same 0.51 mol % overall concentration of all types of defects. Table 1 also lists the peak melting temperatures of rapidly crystallized samples and the average isotactic sequence length calculated as the average *meso* run length (MRL).[10]

Both poly(propylene)s were fractionated via supercritical fluid extraction by the Phasex Co.[33,34] The fractionation was carried out isothermally by increasing pressure in supercritical *n*-propane at 150 °C. Seven fractions were obtained from the metallocene iPP and five fractions from the ZN-iPP. Data relevant to the molecular characterization of the fractions are also listed in Table 1. Sample designations encode, in consecutive order, the following items: catalyst ("M" for metallocene and "Z" for Ziegler−Natta), f for a fraction (no "f" for unfractionated parents), weight-average molar mass in kg/mol followed by "K", and the total number of defects per 100 monomeric units. For example, Mf86K0.56 stands for a fraction obtained from the metallocene iPP with a weight-average molar mass of 86 000 g/mol and with a 0.56 mol % total defect concentration.

Characterization Methods. The molar masses and their distributions were determined by standard gel permeation chromatography using polystyrenes as calibration standards. Melting temperatures and heats of fusion were obtained in a differential scanning calorimeter (Perkin-Elmer DSC-7) using ∼4 mg of sample and a heating rate of 10 °C/min. Static temperature calibration of the instrument was carried out with indium.

The pentad/heptad sequence distributions and the concentration of 2,1 defects were obtained from solution ^{13}C NMR spectra carried out at 125 MHz on ^{13}C using 10 mm o.d. sample tubes. Only methyl resonances were employed in the determination of pentad/heptad sequence distributions. This avoids unwanted contributions from possible differences among nuclear Overhauser effects and relaxation times. Here 15% solutions in tetrachloroethane-1,2-d_2 were used at 125 °C. The pentad/heptad resonance chemical shifts were based on published assignments.[7,8,35−38] The stereodefect concentration was taken

Table 1. Characterization of Parent Polymers and Fractions from Metallocene and ZN-iPP

			defects (mol %)				
sample	M_w (g/mol)	M_w/M_n	stereo	regio	total	T_m (°C)[a]	MRL[b]
M203K0.51 parent	203 900	2.00	0.11	0.40	0.51	155.0	194
Mf86K0.56	86 000	1.43	0.16	0.40	0.56	156.2	176
Mf121K0.50	121 000	1.32	0.11	0.39	0.50	156.3	199
Mf143K0.54	143 000	1.24	0.07	0.47	0.54	156.1	184
Mf200K0.46	200 000	1.23	0.08	0.38	0.46	155.8	216
Mf235K0.45	235 000	1.24	0.07	0.38	0.45	154.6	221
Mf358K0.41	358 000	1.34	0.07	0.34	0.41	154.0	243
Mf383K0.41	383 000	1.47	na[c]	na	na	na	
Z263K0.51parent	262 600	3.19	0.51		0.51	161.4	190
Zf97K1.03	97 000	1.31	1.03		1.03	159.0	91
Zf157Kxxx	157 000	1.27	na		na	na	
Zf163K0.60	163 000	1.97	0.60		0.60	161.3	161
Zf204K0.41	204 000	2.15	0.41		0.41	160.9	239
Zf328K0.36	328 000	1.77	0.36		0.36	162.3	270

[a] Rapidly quenched samples to 25 °C. [b] Average meso run length,[10,21] MRL = $mmmm/[0.5(mmmr + rmmm) + (2,1 \text{ defects})]$. [c] Data not available.

as half the fraction of *mmmr* pentads because any stereodefect sequence will always have two, and only two, associated *mmmr* (=*rmmm*) pentads located at the beginning and the end of each isotactic sequence. Thus, it is possible to determine the total stereodefect population independently of the structures of the various stereodefects.

The average *meso* run length (MRL),[10,21] which represents an average over contiguous *meso* sequences starting at $n = 4$ for $r(m)_n r$, was selected for the characterization of average sequence length of the isotactic components. This definition precludes contributions from short *meso* runs such as ~~~*mmmrmrmmm*~~~ and ~~~*mmmrmmrmmm*~~~, which are most likely not crystallizable but are part of the overall stereodefect distribution. MRL values are listed in Table 1.

X-ray diffraction patterns were recorded in reflection mode at room temperature using a Philips X'Pert PW3040 MRD diffractometer operating at 45 mA and 40 kV. Ni-filtered Cu Kα radiation was used as the source.

Linear growth rates (G) were measured in an Olympus polarized optical microscope used in conjunction with a Linkam hot stage, TP-93. The temperature was controlled with a precision of ±0.1 °C, and the precision of the eyepiece used to measure the spherulitic growth was 0.15 μm. Photographs were also taken during isothermal growth using an Instant Polaroid camera. At any temperature the linearity of the plots of spherulite radius vs time and reproducibility of the measurements were highly satisfactory with regression coefficients higher than 0.99. The measured growth rates were also independent of the position of the spherulite in the specimen and the calculated uncertainty in the value of G was low ($\pm 0.01 \times 10^{-6}$ cm/s).

Overall crystallization rates were taken as the inverse of the time required for 50% of the transformation to take place (similar to the half time rate concept).[39] The degree of transformation, at a fixed isothermal temperature, was followed by the variation of the heat-flow vs time in the DSC-7.

Sample Preparation and Crystallization Procedures. Films approximately 100 μm thick were prepared by compression molding the initial pellets or powders in a laboratory Carver press preset at 200 °C and were used for the microscopic and DSC measurements. Some of the ZN fractions were crystallized at temperatures >120 °C in thermostated oil baths for analysis of crystallographic polymorphs by WAXS. For this purpose, plaques of 1 cm × 1 cm × 0.3 mm were molded, sandwiched between two metal plates covered with thin Al foil, and placed in a vacuum sealed tube to prevent degradation. The tube was immersed in a silicone oil bath at 210 °C for 15 min and then rapidly transferred to another oil bath preset at the required crystallization temperature.

Prior to crystallization in the hot stage or in the DSC, the films were melted at 200 °C for 5 min and cooled at 40 °C/min to the isothermal crystallization temperature. To maximize heat transfer, the DSC was operated in conjunction with an intracooler and under dry nitrogen flow.

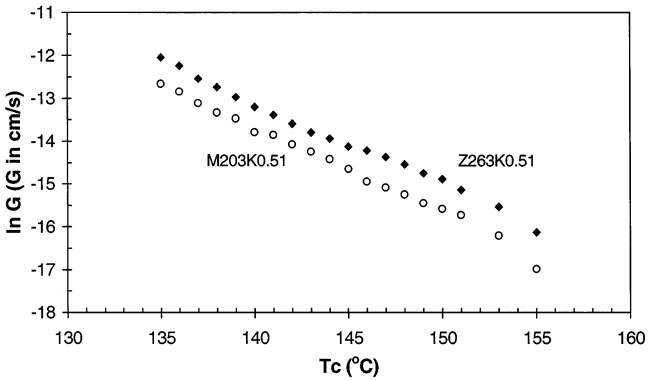

Figure 1. Linear growth rates as a function of crystallization temperature for parents metallocene iPP (○) and ZN-iPP (●) with matched overall concentration of defects, 0.51 mol %.

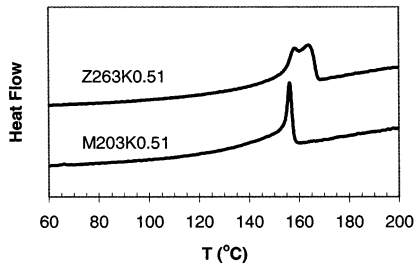

Figure 2. Melting temperatures of parents ZN-iPP (top) and metallocene iPP (bottom). Samples were crystallized at −10 °C/min and melted at +10 °C/min.

Results and Discussion

Comparison of Unfractionated Matched ZN and Metallocene Poly(propylene)s. Before results obtained from the fractions are analyzed in detail, it is also of interest to discuss the differences in melting and crystallization behavior of the unfractionated poly(propylene)s. Isothermal linear growth rates and DSC meltings of the metallocene and ZN parents iPPs are given in Figures 1 and 2, respectively. At any crystallization temperature, the spherulites of the unfractionated ZN-iPP grow at about twice the rate of the metallocene iPP. The DSC melting peak of the ZN-iPP is also considerably broader, multipeaked and shifted to a temperature about 8 °C higher than the melting behavior observed for the metallocene iPP crystallites.

Since the overall concentration of total defects in both poly(propylene)s is the same (0.51 mol %) and both chains are of similar molar mass, the differences in crystallization and melting behavior must reflect a significant difference in distributions of defects. The issue of stereodefects only in the ZN-iPP and stereo- + regiodefects in the M-iPP will be addressed shortly. Previous fractionations of similar industrial-type ZN-iPPs have revealed a nonuniform concentration of defects from chain to chain in these iPPs.[11−14,22−23] Racemic units were found to be more concentrated in the lower molar mass chains. However, the metallocene catalyst with its "single site" nature, leads to iPP chains of narrow molar mass distribution and a narrow distribution of defect concentrations among chains. One consequence of a broad intermolecular distribution of chain defects in the parent ZN-iPP is that it contains a fraction of highly defected molecules that do not participate in the crystallization process. This behavior leads to a lower effective overall defect concentration in the ZN than in the M-iPP. The ZN-iPP contains longer isotactic sequences that will be selected earlier in the crystallization and lead to thicker crystallites, in line with the observed higher growth rates and melting temperatures.

We should also consider if the observed differences in melting behavior between ZN-iPP and M-iPP might be a consequence of a different partitioning of regio vs stereodefects between the crystalline and noncrystalline regions. For example, if the stereodefects more easily enter the crystalline regions than do the regio-2,1-defects, the ZN-iPP chains, with defects only of the stereo-type, will be more crystallizable in line with the results of Figures 1 and 2. This issue has been previously addressed by analyzing the solid state ^{13}C NMR spectra of the crystalline regions of a series of M-iPPs with varied concentrations of stereo- and 2,1-regiodefects.[40,41] Both types of defects were found to enter the crystalline lattice at levels that do not differ significantly. In addition, the similarity of the slopes that characterize the variation of the growth rates with temperature in Figure 1, are indicative of the formation of crystallites with very similar interfacial free energies in both types of iPPs. Hence, we exclude any significant difference in the way stereo- (predominantly a single inversion in configuration shown by the presence of *mmrrmm*) and regio-2,1-defects affect the crystallization of the iPPs used in this investigation.

A confirmation of the predicted interchain microstructure, i.e., homogeneous for the metallocene iPP and inhomogeneous for the Z−N type, will be obtained from microstructural analyses of molecular fractions from both iPPs. The nature of the ZN-iPP inhomogeneous defect distribution as well as a possible nonrandom intrachain defect distribution will be discussed after a detailed analysis of the crystallization rates of the fractions presented in the next section.

Molecular Fractions from Metallocene iPP and Z−N iPP: Fractionation and Analysis of Growth Rates. The molecular characteristics of the fractions obtained from both iPPs by isothermal pressure profile are listed in Table l. This technique allows solvent free recovery of the fractions in adequate quantities for NMR and physical studies.[33,34] With increasing pressure in the fractionation, a systematic increase of the molar mass of the fractions was also observed indicating that the fractionation took place preferentially by molar

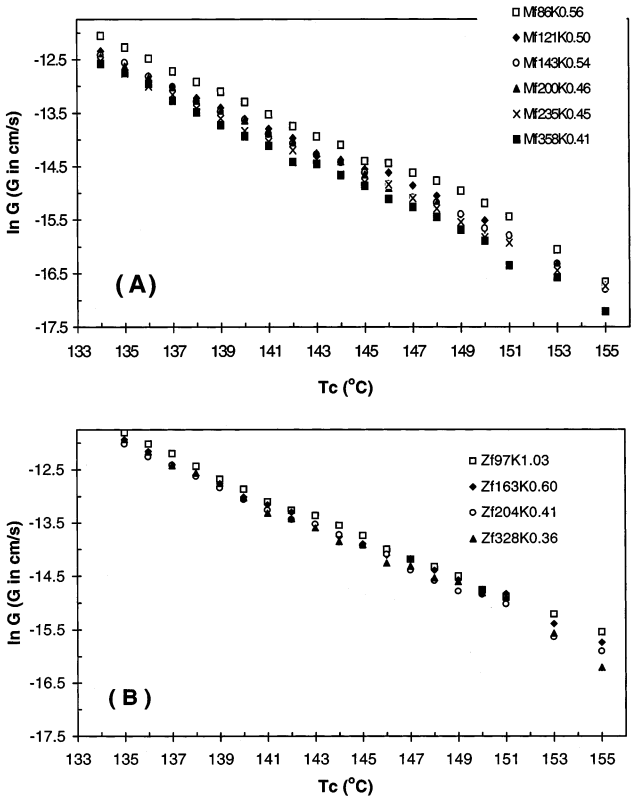

Figure 3. Linear growth rates of iPP molecular mass fractions as a function of crystallization temperature. (A) Fractions from metallocene iPP. (B) Fractions from ZN-iPP. Designation of the fractions follows that given in Table 1.

mass.[33,34] The parent metallocene iPP comprises chains of weight-average molar mass of 204 000 g/mol with the most probable molar mass distribution. From this polymer, seven fractions were isolated with a range in molar mass from 86 000 to 383 000 g/mol and with similar narrow molar mass distributions of 1.3 ± 0.1 in all these fractions. The data are listed in Table l.[42] Of relevance are the very similar concentrations of defects found in all the metallocene fractions, as listed in the fourth and fifth columns of Table 1. A small variation in total defect concentration from 0.56 to ∼0.40 mol % is observed with increasing molar mass. Even so, all of the M-iPP fractions have total defect levels that are very close to the 0.51 mol % observed for the parent M-iPP material. These results offer direct evidence that M-iPP chains have very small intermolecular variations among the concentration of defects and, thus, provide direct experimental basis to conclude that the interchain composition distribution is very narrow in the parent M-iPP. With such a narrow variation in the defect compositional distribution, the metallocene fractions offer an ideal series for analyzing the effects of molar mass on iPP crystallization, independent of the effects of defect content and defect distribution. This analysis will be reported in a subsequent publication.[43]

Well formed spherulites were observed under isothermal crystallization of all the metallocene fractions and the spherulitic linear growth rates, measured in a temperature range between 134 and 155 °C, are given in Figure 3A. Following the dictates of kinetics theories for nucleation and crystallization of polymers,[44,45] the growth rates of all the M-iPP fractions show a similar variation with undercooling, i.e., a decrease of the rate by about 100 times with increasing crystallization

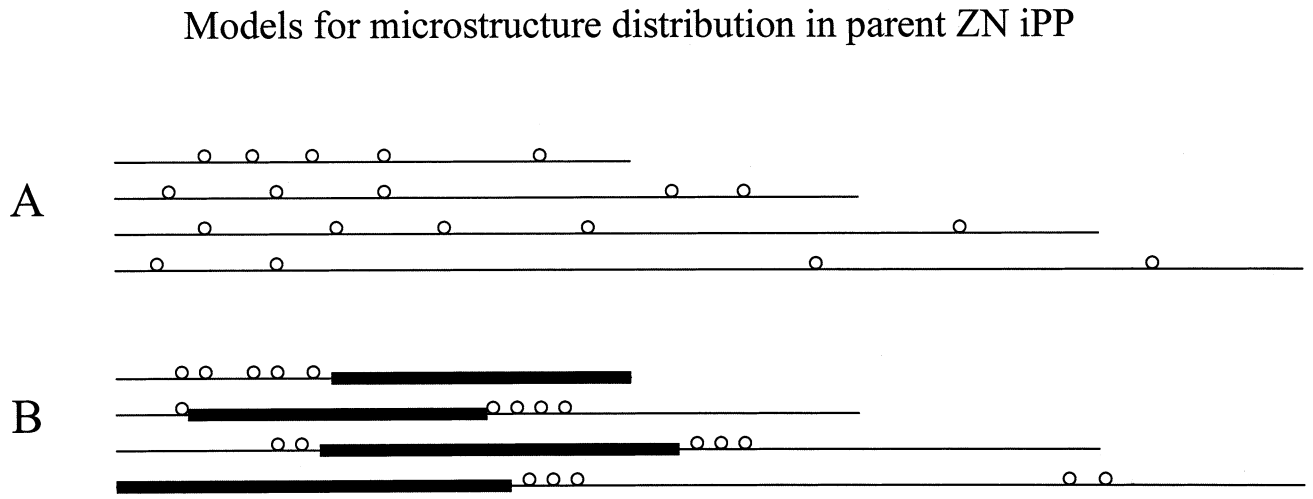

Figure 4. Two possible microstructural models of stereosequence distribution in the parent ZN-iPP. (A) The concentration of defects is nonuniform between the molecules and randomly distributed intramolecularly. Increasing concentration of defects is correlated with molar mass. Different lengths of crystallizable sequences are found. (B) The concentration of defects is also nonuniform between the molecules but the intramolecular distribution of defects is blocky. Long similar crystallizable sequences, highlighted for visual effect, are found in all the chains.

temperature in the range analyzed. In addition, the effect of molar mass is reflected by about a one-half decrease of the rate with increasing molar mass at any temperature. For example, at a crystallization temperature of 140 °C growth rates values (in cm/s) of 1.68×10^{-6}, 1.23×10^{-6}, 1.20×10^{-6}, 1.19×10^{-6}, 0.98×10^{-6}, and 0.89×10^{-6} were obtained for a molar mass change from 86 000 to 358 000 g/mol. This difference is not large, but it is, however, systematic and much larger than the estimated experimental error in the measurement of the growth rate.

A small molar mass dependence of the growth rate is qualitatively similar to that reported for linear polyethylene and for other homopolymers when crystallization takes place at high undercoolings.[45−52] For example, linear polyethylene displays a discrete maximum in the crystallization rate with molar mass for undercoolings lower than 30°. However, at higher undercoolings, the maximum is not observed, and the change of the rate with molar mass is less pronounced, becoming very small at the highest undercoolings. The crystallization of the metallocene iPP fractions takes place at undercoolings well above 30°. Hence, the small molar mass dependence of the growth rate, which is observed in Figure 3A, fits the pattern of other homopolymers and copolymers.[45−52] The linear growth rates of the metallocene fractions follow the expected variation for chains of different lengths with very similar contents of defects and the same random intramolecular distributions of defects.

The natural logarithm of the experimental linear growth rates (G) of the ZN-iPP fractions are given in Figure 3B for a range of crystallization temperatures between 135 and 155 °C. The x and y axes of this plot are identical to the axes in the plot of growth rates of the metallocene fractions (Figure 3A). This consistency facilitates a comparative study. In analyzing the data of Figure 3, parts A and B, we notice smaller but still significant differences in the growth rates of the ZN-iPP fractions, when compared to those of the metallocenes. No systematic variation of G with either molar mass or concentration of defects is found in the ZN-iPP fractions. In principle, this is an unusual result because a strong effect of the concentration of defects in lowering G was reported for metallocene iPPs of a fixed molar mass.[19] The same variation with defects was also found in other M-iPP fractions for which the details of the fractionation were not provided.[16] Therefore, in the range of defect concentrations of the ZN-iPP fractions, one would have expected a significantly lower G for the fraction with 1.03 mol % defects than for the fraction with 0.36 mol % defects. The data of Figure 3B show that this is not the case; in fact, there are only minor differences between the growth rates of the ZN-iPP fractions at a fixed crystallization temperature. The differences in crystallization behavior, when compared to the metallocene fractions, likely reflect significant differences in the distributions of defects.

The molar mass and concentration of defects of the fractions obtained from the ZN-iPP, also listed in Table 1, confirm the inhomogeneous interchain concentration of defects of the parent polymer. As the molar mass of the fractions increases from 97 000 to 328 000 g/mol, the total defect content decreases from 1.03 to 0.36 mol % respectively. This inverse relation between chain length and concentration of defects was also observed in ZN-iPP fractions obtained by a solvent−nonsolvent extraction fractionation procedure[11,12] and in fractions obtained by TREF.[14,22,23] Hence, quite different types of fractionation studies reveal an interchain variation of the concentration of defects in the ZN parent that decreases as the molar mass increases. Neither the fractionation nor characterization data reveal any details about the intramolecular distribution of defects. The molecular characteristics of a defect distribution are probably best addressed by indirect studies of properties that relate to an intramolecular defect distribution. In this context, different possible scenarios are viable and schematics for two of these models for the crystalline chains are given in Figure 4. A third composite model that results from applying a three-state statistical model to the observed NMR pentad/heptads stereosequences will be discussed in detail in the second part of this series.[31] The results of this model are summarized in the last section of the present paper.

In Figure 4A, a defect distribution is shown that is nonuniform on an intermolecular basis, but the intramolecular defect distribution is random. According

to this model, the defect concentrations increase continuously with decreasing molar mass. The crystallization behavior of fractions from this model is expected to be proportional to the average defect composition in the melt which changes among the fractions. Therefore, after fractionation, much lower crystallization rates are expected for the fractions of lower molar mass because, on average, they comprise a higher concentration of defects and shorter isotactic sequences than the less defected fractions.[16,17,19,40] The second possibility (depicted schematically in Figure 4B) is a microstructural model in which the intermolecular defect composition is also nonuniform with the shorter chains having a higher concentration of nonisotactic units. However, in this model the intramolecular distribution of defects is blocky (nonrandom) with long runs of crystallizable isotactic sequences being present in all chains. On average, the second model has similar types of long crystallizable sequences present in all of the chains. It is clear that the crystallization behavior of fractions from this second model will be quite different from the behavior of fractions in the first, which has a random intramolecular defect distribution. In the second model, the overall concentration of defects also changes from chain to chain but the crystallization is led by the long isotactic blocks. The concentration of short, less crystallizable isotactic sequences is minimal compared to the concentration of these sequences in the first model. The crystallization behavior of the fractions from the second iPP model should be similar to the crystallization of a diblock copolymer in which one of the blocks is noncrystallizable.

If the actual ZN defect distribution follows the microstructural model given in Figure 4A, one would expect, after fractionation, that a similar crystallization rate should be observed for both the metallocene and the narrow ZN fraction with matching defect concentrations. After fractionation, the overall defect concentration will be much closer to the single molecule concentration in both iPPs. A difference in crystallization behavior, however, is maintained as seen in Figure 3, parts A and B, where the growth rates of fractions Mf358K0.41 and Zf204K0.41 are compared. The spherulites of the Ziegler fraction grow more rapidly than those of the metallocene counterpart. This reaffirms the idea that, even after fractionation, the Ziegler fractions contain longer isotactic sequences; put in another way, the broad defect distribution of the parent ZN-iPP is sustained to some extent in the fractions. Moreover, the fact that the growth rates of all the Ziegler fractions are so similar also indicates that the intramolecular distribution of the defects in the ZN fractions is different from that of the metallocene fractions. The similarity of the rates in Figure 3B suggests that the same nonrandom intramolecular distribution is propagated along all the molecules of the parent ZN-iPP. In other words, the defect distribution of the ZN-iPP does not conform with the microstructure modeled in the scheme of Figure 4A.

The ZN fraction with the highest concentration of defects is also the fraction of the lowest molar mass. Thus, one could argue that the expected decrease of G with increasing defect content in the ZN fractions may be compensated by an opposite effect of molar mass on G, as demonstrated in the metallocene series. If this were the case, model 4A could still apply to describe the defect distribution of the ZN-iPP. To probe this possibility, the growth rate data of the lowest molar mass ZN fraction with 1.03 mol % defects were corrected to the values that this fraction would have if its molar mass is ~200 000 g/mol. To make this correction, data obtained for the metallocene fractions, shown in Figure 3A, are appropriate because they purely reflect the variation of G with molar mass independently from the effect on the rate of the defect concentration. Thus, the growth rate data of the fraction Zf97K1.03 were lowered by the difference in G given by the metallocene fractions in a range between 97 000 and 204 000 g/mol taken from Figure 3A. The corrected G data for the 1.03 mol % fraction (closed diamonds) and the uncorrected one for fraction Zf204K0.41 of low defect content (open circles) are plotted in Figure 5. The data are also compared with published growth rate data of a metallocene iPP with 1.0 mol % of defects,[19] given by the solid line in this figure. It is evident that the correction for molar mass has very little effect on the variation of G among the ZN fractions. The growth rates of the ZN fractions fall on the same line, which is positioned much higher than that expected had the defects been randomly distributed as is the case for the data of the metallocene iPP with the same 1.0 mol % defects of Figure 5.

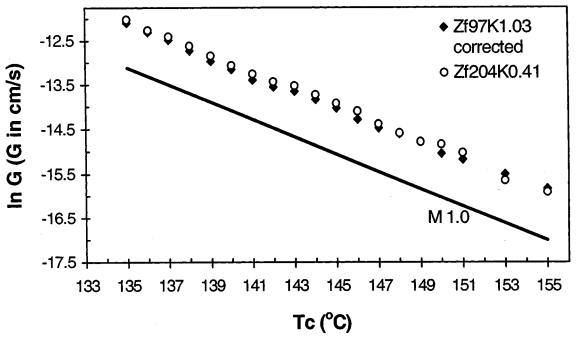

Figure 5. Linear growth rates of ZN fraction Zf97K1.03 corrected for the effect of molar mass on the rate (◆) compared with growth rates of ZN fraction Zf204K0.41 (○). The continuous line indicates the variation of growth rates with temperature of a metallocene-type iPP with 1.00 mol % of defects extracted from ref 19.

The similarity of the growth rates of all the ZN fractions, even after correction for different molar masses, provide evidence that suggests that the intramolecular defect microstructure of the parent ZN-iPP, as well as the fractions, could be blocky. Even after careful fractionation, the ZN-iPP growth rates are considerably higher than observed for the metallocene fractions. These observations offer additional evidence for the possible blocky nature of the ZN-iPP. As will be shown below in this work, the lack of formation of the γ polymorph, which requires short isotactic sequences, also rules against model 4A. Hence, the results of the growth rates favor the microstructural model shown in Figure 4B.

Additional evidence, which supports the stereoblock defect microstructure of the ZN-iPP chains, is found in the WAXS diffractograms obtained in the two most defected ZN fractions. We have previously reported that a metallocene iPP with a concentration of 1.0 mol % of homogeneously distributed defects, crystallized at 125 °C, develops about half of the crystallites in the γ polymorph and the other half in the α monoclinic form.[21] It was also observed in our previous work that the percentage of γ phase developed by two unfractionated

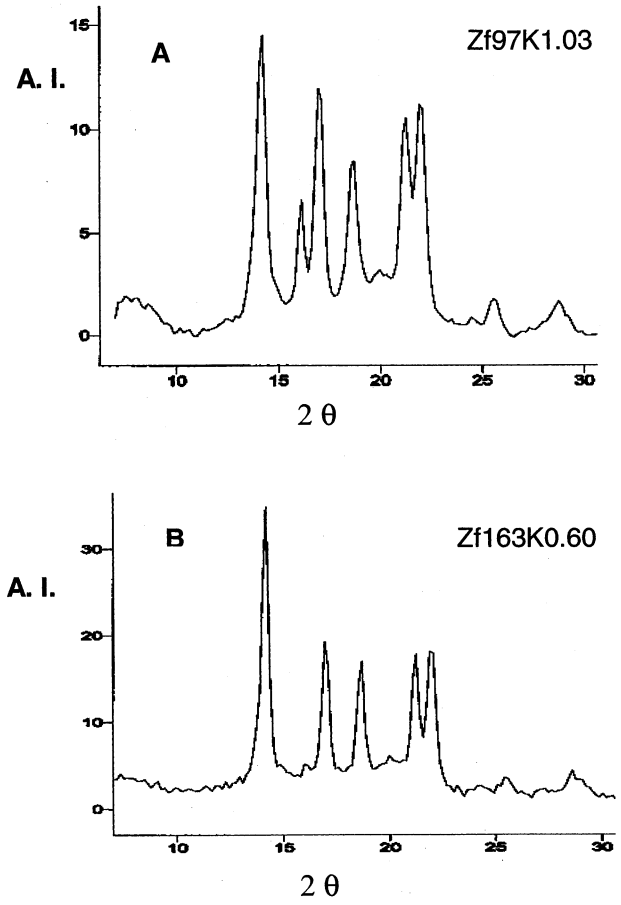

Figure 6. WAXS diffractograms of ZN-iPP fractions Zf97K1.03 and Zf163K0.60 collected at room temperature after 3 days of crystallization at 125 °C.

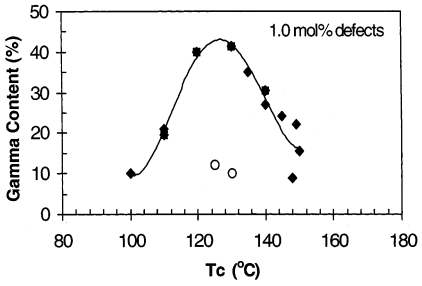

Figure 7. Variation of the concentration of the γ polymorph with crystallization temperature for different iPPs with matched 1.00 mol % overall defect concentration: (◆) metallocene type iPP (data from ref 21); (○) ZN-iPP fraction Zf97K1.03.

ZN-iPPs was, at any temperature, below the level of detection of this polymorph by WAXS. The low γ content was attributed to the broad defect distribution of the ZN-iPPs.[21] The WAXS diffractograms of the two most defected ZN fractions crystallized at 125 °C are shown in Figure 6A for Zf97K1.03 and in Figure 6B for Zf163K0.60. The intensity of the reflection at a 2θ of 20°, characteristic of the γ polymorph, is low and corresponds to less than 10% in both fractions. The peak at $2\theta = 16°$ is associated with the β polymorph, more abundant in the lower molar mass fraction. In Figure 7, the percentage of the γ phase obtained for the Zf97K1.03 fraction is compared to the γ form developed with increasing temperature by a metallocene iPP with matched concentration of defects. The content of γ phase developed by the ZN fraction is four times lower than the value of the metallocene iPP with its narrow defect distribution. It is basically constant in the range of temperatures studied. Hence, we find that at a matched overall concentration of defects of 1.0 mol %, the structural requirements for the formation of the γ polymorph are present in the metallocene iPP, but they are basically absent in the ZN fraction. These requirements were described in detail in our previous work[21] and are summarized in the following two major points: 1. Chains whose microstructure leads to thin crystallites must be present; i.e., there must be short crystallizable isotactic sequences available. 2. There must be a structure that prevents folding in the crystal amorphous interfacial region and requires tilted ordered chains to propagate a lamellar crystallite. The lamellar propagation is favored by a tilted antiparallel molecular arrangement of the γ crystallographic phase.[53,54] As seen in Figures 6 and 7, even after crystallization in a temperature range that is most favorable for the formation of the γ phase,[21] the content of γ phase obtained in the ZN fractions is much lower than that expected for a chain with a random defect distribution. The most characteristic reflection of the γ form, that at a 2θ of 20°, is almost absent from both diffractograms. This result is expected for a molecule where long isotactic sequences join blocks of poorly stereoregular sequences, such as those of the ZN stereoblocky type described schematically in Figure 4B.

From the relation between the maximum content of γ form and the concentration of defects in narrowly distributed metallocene iPPs, given in Figures 8 and 9 of ref 21, we find that 12% of the γ polymorph corresponds to an average *meso* run length (MRL) of 220 repeat units. This value is considerably larger than the average MRL of 91 units for the ZN-iPP fraction with 1.03 mol % defects and suggests that contiguous isotactic sequences of at least 220 units must be present in the Zf97K1.0 fraction in a relatively high concentration. As presented in next section, a modified Busico three-state model leads to a distribution of sequence lengths for this fraction consistent with these data. Long isotactic runs favor the formation of folded-chain crystallites in the ZN fractions and, hence, they crystallize preferentially in the α polymorph. In a recent publication,[27] the analysis of the polymorphic behavior was also taken as an indirect measure of the degree to which the defects in the iPP chain deviate from a random distribution.

Overall Crystallization Rates. Previous parallel or independent studies of the linear growth rates and the overall crystallization rates measured by dilatometry or by differential scanning calorimetry of linear polyethylene fractions and other types of homopolymers, have resulted in an identical temperature coefficient.[44,46,55,56] In addition, these methods of measurement give identical variation of the rates with molar mass or with concentration of defects. Hence, data from either growth rates or overall rates have been used to test for conformity with kinetic theories of polymer nucleation and growth.[44,46,51,52] We were also interested in testing if the overall crystallization rates measured by DSC follow the behavior observed by the growth rates of the parent iPPs and their fractions. Furthermore, the overall crystallization rates apply more directly to the solidification rates used in industrial processes because the data that characterize these rates are mass or volume-based quantities, and the measurements are not

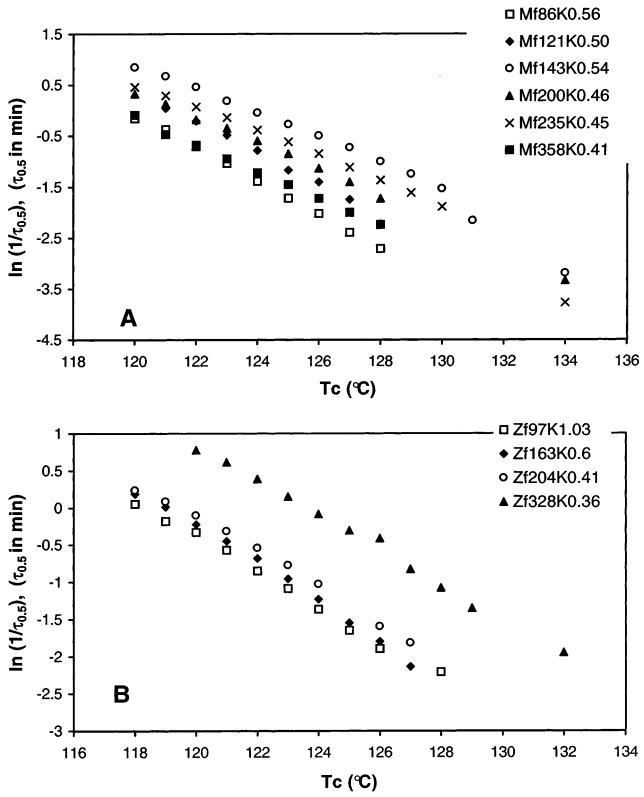

Figure 8. Overall crystallization rates of iPP molecular fractions as a function of crystallization temperature. (A) Fractions from metallocene iPP. (B) Fractions from ZN-iPP. Designation of the fractions follows that given in Table 1.

limited to having to observe a specific morphological feature as in microscopic methods.

The natural log of the inverse of the time required to obtain 50% of the total transformation ($\tau_{0.5}$), taken at the peak of the exotherms, is plotted vs crystallization temperature in Figure 8A for the metallocene fractions, and in Figure 8B for the ZN fractions. Different features are apparent from these plots. At a fixed crystallization temperature, the variation of the overall rate among the metallocene fractions is not systematic with molar mass as was observed with the growth rates. The variation of the overall rates of the ZN fractions is also different from the behavior observed for the growth rates in Figure 3B. At any temperature, the overall crystallization rate of the less defected ZN fraction (Zf328K0.36) is about three times faster than the rate of any of the ZN fractions. The difference in overall rates between the more defected ZN fractions, although small, is directly related to their concentration of defects. For example, it is the fraction with the highest concentration of defects (of the lowest molar mass) that shows the lowest overall rate.

These results can be explained by variations among the nucleation densities found in the fractions and parent iPPs. The number of spherulites that develop in each specimen were measured at selected crystallization temperatures. The data of the parent metallocene iPP and its fractions will be reported first. Figure 9 shows micrographs of the parent metallocene and selected fractions crystallized at 134 °C for approximately the same lengths of time. The spherulites are not uniformly distributed in most of the fractions and their rapid appearance and high numbers are indicative of a nucleation enhanced by some external agent. As seen in Figure 10, parts A and B, for five representative temperatures, the number of nuclei in a fixed volume follow the molar mass with the same random pattern as the overall crystallization rate. The latter is governed by the rate of nucleation, as demonstrated in the crystallization of many polymeric systems.[44,45,55,57,58] Consequently, the fractions with a higher nucleation density will yield a fixed level of crystallinity faster than fractions in which fewer nuclei are formed, regardless of the magnitude of the spherulitic linear growth rate. The solid lines in these figures follow the experimental data and are only intended as a guide to the eye. They do not represent any theoretical functionality.

Nucleants were not added to the parent metallocene or ZN polymer, inferring that what causes enhanced nucleation must be acquired either in the polymerization or the fractionation process. About 0.1% of the antioxidant Irganox 1010 was added to the *n*-propane before fractionation. However, as seen in Figure 10A, the parent metallocene iPP, free of this antioxidant, shows as high a nucleation density as the highest observed value among the fractions. From this, we conclude that the antioxidant, which could have been randomly distributed during fractionation is not nucleating the metallocene fractions. Since significant amounts of MAO are used as cocatalysts during polymerization, this agent or residues from the metallocene catalyst may enhance the nucleation rate of the metallocene iPP and its fractions.

Significant differences in the nucleation density of the ZN-iPP fractions are also observed. Representative micrographs of the lowest and highest molar mass ZN fractions are given in Figure 11. The nucleation density of the highest molar mass fraction is over 1 order of magnitude higher than any other ZN fraction. Nucleation densities and overall crystallization rates for the ZN fractions are shown in Figure 12, parts A and B, respectively, as a function of molar mass, for representative crystallization temperatures. Following the nucleation density pattern, the overall crystallization rates show a small increase with molar mass up to 200 000 g/mol and a large increase for the higher molar mass fraction. For example, at a crystallization temperature of 123 °C, the rate changed from 0.34 to 0.46 min^{-1} for defects changing from 1.03 to 0.41 mol % and to 1.16 min^{-1} for the less defected, highest molar mass fraction. Thus, as seen in Figure 12B, the variation of the logarithm of the rate is not linear with increasing molar mass or decreasing concentration of defects. The highest molar mass, low defected fraction shows a significantly higher rate. We ruled out that catalyst residues may be causing the high rates of the ZN fraction. Large contents of cocatalyst residues are not an issue in the polymerization with ZN catalysts. Moreover, statistical models[27] predict a fraction of very long, highly isotactic molecules in ZN-iPP, which naturally will be concentrated in the higher molar mass fraction. It is reasonable that these very long, highly isotactic molecules (absent in the metallocene iPP) may persist in the melt as aggregates and lead to a significant enhancement of the nucleation and crystallization rates. Melt memory effects have been observed previously in the crystallization of iPP[59] and were also tested in the ZN fraction Zf328K0.36. A small decrease of the overall crystallization rate at 124 °C was found by increasing the melt residence time at 200 °C from 5 to 30 min, but higher melt temperatures, such as 250 °C, could not be tested

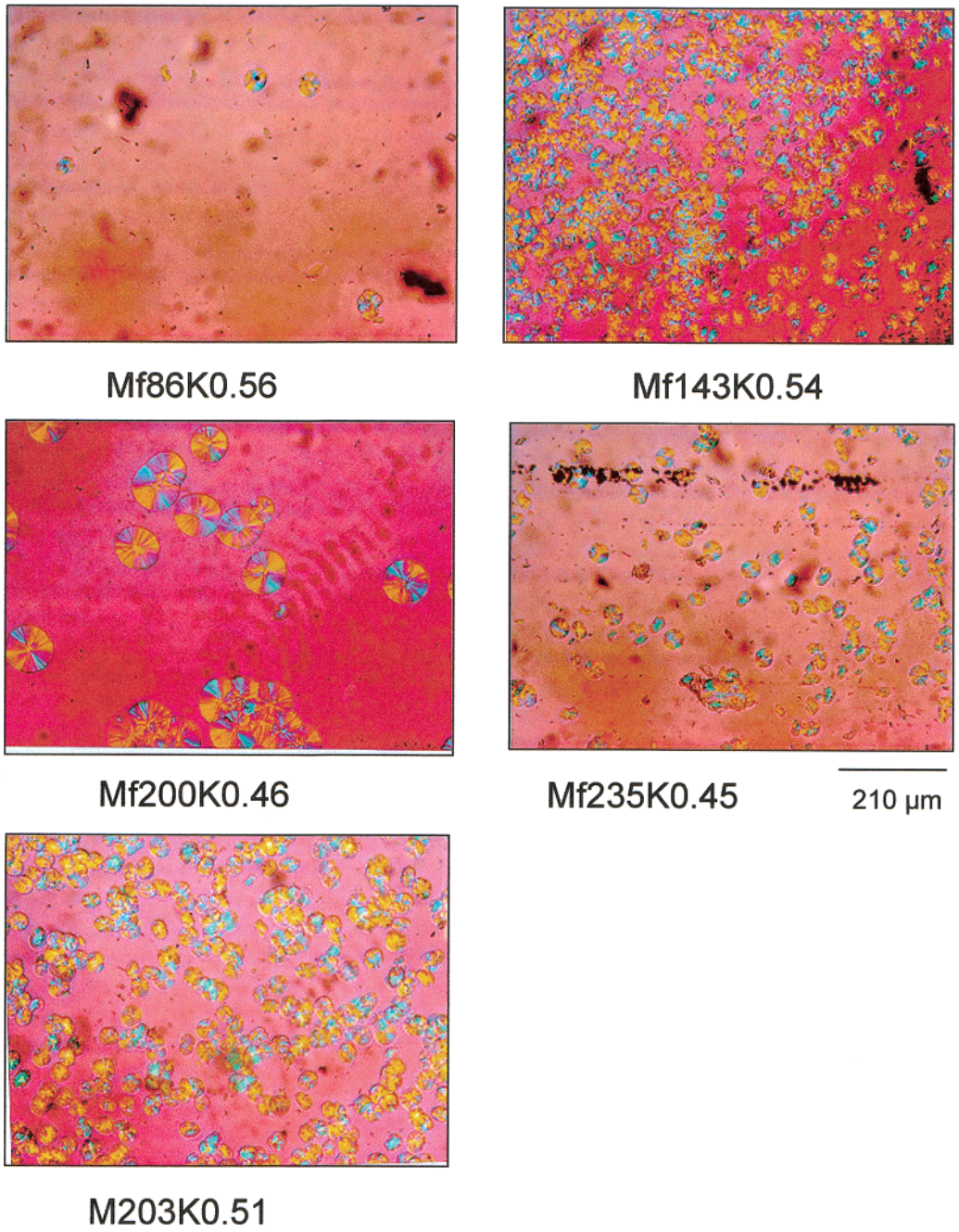

Figure 9. Polarized optical micrographs of the parent metallocene iPP and selected fractions isothermally crystallized at 134 °C for Mf86K0.56 (7 min), Mf143K0.54 (7 min), Mf200K0.46 (9 min), Mf235K0.45 (7 min), and M203K0.51 (7 min).

because the sample degraded. The concentration of very long, highly isotactic molecules is more diluted in the parent ZN-iPP and the lower molar mass fractions in agreement with their observed lower nucleation rates. Thus, the overall crystallization rate of the parent ZN-iPP and all the fractions, except the one with the higher molar mass, are very similar, in line with the similar growth rates observed in these fractions and in agreement with their blocky defect microstructure.

From the crystallization behavior of the two most general types of iPPs, we can postulate two different types of factors acting as "precursors" of the overall crystallization, i.e., catalyst residues and the very long chains present in the ZN-iPPs. These factors affect primary nucleation and, therefore, the overall crystallization rates characteristic of each fraction. Thus, it is not surprising that a correlation between the overall crystallization and microstructural variables is not found in the ZN-iPPs of this study. On the other hand, the linear growth rates which are independent of the primary nucleation rate and led by a process of secondary nucleation,[44] offer a better tool to correlate with the structural variables of the poly(propylene) chain. These results indicate that caution must be exercised when using overall crystallization rates to correlate physical properties with molecular microstructure. Any other mass or volume based measurement of the crystallization of iPP, such as optical or X-ray scattering may be subjected to the same type of enhanced nucleation described in this work.

Experimental NMR Stereosequences. Modified Busico Three-State Statistical Model. The defected pentads and heptads observed by ^{13}C NMR for the ZN-iPP fractions and the parent ZN-iPP are listed in

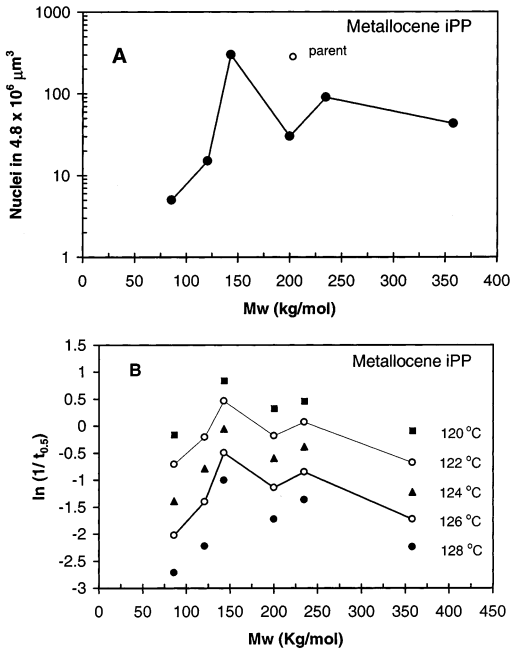

Figure 10. A. Variation of the nucleation density with molecular mass for fractions (●) and unfractionated metallocene iPP (○) crystallized at 134 °C for ∼7 min. B. Overall crystallization rate as a function of molecular mass for metallocene iPP fractions crystallized at the indicated isothermal temperatures.

Table 2. In agreement with previous studies,[7−11,22−26] we notice a nonnegligible concentration of purely syndiotactic sequences (*rrrrrr*) in all the ZN fractions, including the fraction with the highest molar mass. In addition, stereoerrors of the type, *rmrrrm* or *rmrrrr* are also not detected.[25] The presence of the *mrrrmm* heptad indicates that isotactic blocks of opposite handedness are present. The most abundant defect consists of a single opposite configuration, ∼0001000∼, and is detected by the *mmrrmm* heptad. There are also more defective (*mmrrmr*) defects connecting isotactic blocks in all the ZN fractions as indicated by the normalized integrals corresponding to the steric pentads and heptads listed in Table 2.

The experimental pentad/heptads stereosequences were fit with two and three state statistical models. The predicted sequence length distributions will be discussed in detail for conformity to the observed fractionation and crystallization rates in the subsequent paper.[31] The value in fitting an observed pentad/heptad distribution with any statistical model is that the results can be used to identify the molecular component that gives rise to the various types of stereodefects. None of the models led to a defect distribution resembling the schematic microstructural model represented in Figure 4B, which most closely adheres to the experimental data. This blocky distribution of defects is difficult to propose with the classical two or three state statistical models because conceptually it would require switches between enantiomorphic (Es) and chain end control (CE) sites. The results obtained with the modified Busico three-state model are of relevance; therefore, they are also presented here. In the original work by Busico et al.[25] the ZN-iPP chains are modeled as a mixture of three types of molecules using a three-state statistical model. For a late generation, but weakly isotactic, Ziegler−Natta poly(propylene), the result was a mixture of very high isotactic molecules produced by an Es state, poorly isotactic or atactic molecules produced by a CE state and isotactic molecules produced by switching between two Es control sites (*C1*), each leading to different isotacticity levels.

As mentioned earlier, the only change made in Busico's original three-state model was to employ first-order Markovian statistics for the symmetric chain (termed CE in Busico's work, now referred to as CE1) component as opposed to the Bernoullian statistics used in the original Busico three-state model. The enantiomorphic Es and switching *C1* states were used exactly as represented by Busico and co-workers.[25] This modified model presents the unfractionated ZN-iPP as a composite of chains of different lengths in which molecules of the same length can have different concentrations of randomly distributed defects in two components (from Es and *C1* chains) and nonrandom defects in the third, CE1 chain component. The composite leads to a result where the defect concentration will decrease with increasing molar mass in agreement with the fractionation data. The most significant result obtained from fitting the modified Busico three-state model to the observed ZN-iPP pentad/heptad fraction data is that the three states are found to have similar compositions and similar sequence distribution curves in all four ZN-iPP fractions. It is only the relative amounts of each component that is predicted to change from fraction to fraction with increasing molar mass. The presence of very long isotactic sequences, predicted in the nonrandom CE1 component, is also important. This result may lead to similar growth rates as observed for the ZN-iPP fractions. During slow crystallization, highly isotactic Es molecules and long isotactic sequences from the CE1 component will be selected first and at about the same rate for all the fractions. This is inferred from the

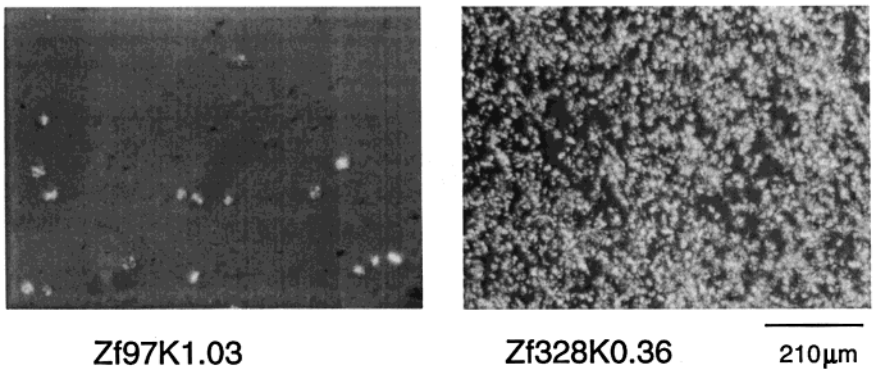

Figure 11. Polarized optical micrographs of fractions Zf97K1.03 and Zf328K0.36 isothermally crystallized at 134 °C (3 min)

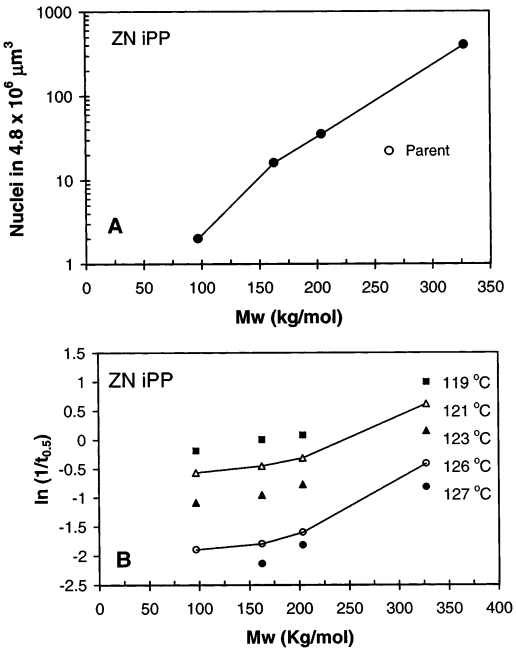

Figure 12. A. Variation of the nucleation density with molecular mass for fractions (●) and unfractionated ZN-iPP (○) crystallized at 134 °C for 3 min. B. Overall crystallization rate as a function of molecular mass for ZN-iPP fractions crystallized at the indicated isothermal temperatures.

>0.994 isotactic sequence probability of the Es component predicted for all the fractions.[31] The concentration of the less isotactic CE1 component was found to increase in the fractions of lower molar mass. However, the effect of this dilution on the crystallization of the Es component is predicted to be small and possibly compensated by differences in molar masses between the fractions. Therefore, the predicted crystallization behavior conforms to the experimental observations. In addition, most of the crystallizable sequence lengths predicted by the ES/*C1*/CE1 model are over 200 isotactic units in agreement with the small contents of the γ polymorph that are observed. Homogeneously distributed metallocene iPPs with average meso run lengths of ~200 units and higher, led to contents of the γ polymorph of less than 20%.[21] Thus, it is expected that a nonrandom, "stereoblocky", defect distribution of the most populated CE1 type molecules of the lowest molar mass fractions (Zf328K0.36 and Zf163K0.60), would crystallize with an even smaller content of this polymorph, in agreement with the experimental observations.

A similar pentad/heptad analysis of the stereosequences in the parent M-iPP and its fractions revealed only one principal stereodefect and that was *mmrrmm*, which is the defect that consists of a single opposite configuration. At the same level of NMR sensitivity used for the ZN-iPP fractions, the *rmmr*, *mmrm* + *rrmr*, and *rmrm* pentads and the various *rr* centered heptads, other than *mmrrmm*, were below the experimental NMR noise level in the metallocene iPPs. This result is predicted by a single state, enantiomorphic site control (Es) model[10] and is consistent with the behavior of a single sited catalyst. In addition to *mmmm*, the only other significant methyl resonances observed are *mmmr* + *rmmm*, *mmrr* + *rrmm*, and *mmrrmm*, which are expected in a 2:2:1 ratio, as observed for the M-iPP parent and its fractions. This stereodefect, which arises from a single configurational error, accounts for virtually all of the stereodefects in M-iPP and comprises about 20% of the total defect distribution. The stereodefect distribution is, therefore, Bernoullian[1] and consistent with the linear growth rate data obtained from the metallocene series, which does not support any significant grouping of regio- or stereodefects. In fact, iPP prepared with "single sited" metallocene catalysts have been shown in independent studies to display uniformly distributed stereo- and regiodefects.[1,60]

Concluding Remarks

The crystallization behavior of a metallocene and a ZN-iPP with the same molar mass and same overall concentration of defects was studied in relation to their defect microstructure. Conclusions with respect to inter- and intramolecular distribution of the defects in each type of iPP were possible from the analysis of the crystallization data of their molecular fractions, which were obtained by isothermal pressure profile in supercritical *n*-propane.

The fractions from the metallocene iPP provide direct, supporting evidence of the "single sited" nature of the catalyst. They display a range in molar mass but the same defect concentrations, which indicate the presence of uniform intermolecular defect concentrations in the parent metallocene iPP. The experimental linear growth rates of the fractions were those expected for chains with a random intramolecular distribution of defects. The variations of these rates with molar mass reflect their different number of entanglements per chain in the melt.

The overall crystallization rates of the parent metallocene iPP and its fractions are affected by an enhanced

Table 2. Stereosequence Distribution of Unfractionated ZN-iPP, and Its Fractions

		distribution				
sequence	assignment, ppm (TMS)	Z263K0.51 parent	Zf97K1.03	Zf163K0.60	Zf204K0.41	Zf328K0.36
mmmm	21.8	0.9632	0.9357	0.9683	0.9766	0.9802
rmmm	21.55	0.0102	0.0205	0.0120	0.0082	0.0073
rmmr	21.33	0.0029	0.0016	0.0016	0.0010	0.0008
mmrr	21.02	0.0113	0.0200	0.0099	0.0073	0.0057
mmrm + *rrmr*	20.79	0.0034	0.0036	0.0013	0.0014	0.0011
rmrm	20.55	0.0009	0.0008	0.0001	0.0005	0.0004
mrrrrm	20.33	0.0006	0.0013	0.0003	0.0003	0.0003
mrrrr	20.3	0.0007	0.0016	0.0003	0.0002	0.0004
rrrrr	20.25	0.0014	0.0036	0.0007	0.0008	0.0012
rmrrrm	20.17	0.0000	0.0000	0.0000	0.0000	0.0000
rrrrmr	20.13	0.0012	0.0016	0.0006	0.0005	0.0004
mmrrrr + *mmrrrm*	20.06	0.0009	0.0023	0.0007	0.0005	0.0003
rmrrmr	20	0.0000	0.0000	0.0000	0.0000	0.0000
mmrrmr	19.93	0.0008	0.0014	0.0006	0.0004	0.0003
mmrrmm	19.85	0.0035	0.0062	0.0034	0.0026	0.0019

nucleation, probably caused by catalysts or cocatalyst residues. Thus, the rates follow the variation of nucleation density in each fraction, and a correlation between these measurements and the defect microstructure of the metallocene iPP, or its fractions, is not possible.

The molar fractions obtained from the ZN-iPP confirmed that the defect composition is broadly distributed on an intermolecular basis. Thus, while the molar mass of the fractions varied from 97 000 to 328 000 g/mol, the concentration of defects decreased from 1.03 to 0.36 mol %. In addition, the basically identical growth rates obtained in all the ZN fractions and the lack of formation of any significant content of the γ polymorph, even in the most defected fraction, is consistent with a blocky intramolecular nature of the defects in the ZN-iPP molecules. The data are also consistent with a microstructural model in which most of the crystalline chains comprise long runs of basically defect free isotactic units followed by runs of other less isotactic or atactic sequences.

Very similar overall crystallization rates were also found for most of the ZN fractions, which suggests a blocky microstructure. However, the highest molar mass fraction displayed much higher nucleation density and, thus, higher overall crystallization rates than the rest of the fractions. This could be attributed to the presence of aggregates in the melt from the higher concentration of molecules with very high molar mass in this fraction. These long, highly isotactic molecules are not found in the narrowly distributed metallocene iPP.

As a consequence of the enhanced nucleation caused either by foreign particles (possible catalyst residues) in the metallocene iPP, or by possible aggregates in the melt induced by the long chains of the ZN-iPP, a correlation between the overall crystallization and their microstructural variables may not be found. The linear growth rates, which do not depend on primary nucleation, were adequately correlated with molar mass in fractions from the metallocene iPP, with uniform distribution. The growth rates also served as a useful tool to infer an intramolecular, nonrandom distribution of defects in the ZN-iPP chain.

A multistate statistical model of the ZN-iPP microstructure predicts in all molar mass fractions the same three types of molecules, almost defect free isotactic chains, mainly isotactic molecules with non-Bernoullian defect distribution, and poorly isotactic molecules. The defect concentration and sequence distribution of the three types of molecules is the same in all ZN-iPP fractions, differing only in their relative amounts. This model was found to be consistent with the fractionation results and growth rates of the ZN fractions.

Acknowledgment. This work was supported by the National Science Foundation Polymer Program (DMR-0094485). The authors acknowledge useful comments on this work by Prof. L. Mandelkern. Eric Ritchson, a REU chemical engineering student, and Dongsheng Li are also acknowledged for helping with the DSC experiments and collecting the WAXS diffractograms. We are also grateful to Charles Ruff of the ExxonMobil Co. for NMR data. J.A.B. acknowledges partial support from the Fundacion Repsol YPF.

References and Notes

(1) Brintzinger, H. H.; Fischer, D.; Mülhaupt, R.; Rieger, B.; Waymouth, R. M. *Angew. Chem., Int. Ed. Engl.* **1995**, *34*, 1143.
(2) Fischer, D.; Mülhaupt, R. *Macromol. Chem. Phys.* **1994**, *195*, 1433.
(3) Zambelli, A.; Locatelli, P.; Bajo, G.; Bovey, F. A. *Macromolecules* **1975**, *8*, 687.
(4) Zambelli, A.; Locatelli, P.; Provasoli, A.; Ferro, D. R. *Macromolecules* **1980**, *13*, 267.
(5) Kawamura, H.; Hayashi, T.; Inoue, Y.; Chûjô, R. *Macromolecules* **1989**, *22*, 2181.
(6) Busico, V.; Corradini, P.; De Martino, L.; Graziano, F.; Iadicicco, A. M. *Makromal. Chem.* **1991**, *192*, 49.
(7) Busico, V.; Corradini, P.; De Biasio, R.; Landriani, L.; Segre, A. I. *Macromolecules* **1994**, *27*, 4521.
(8) Busico, V.; Cipullo, R.; Corradini, P.; Landriani, L.; Vacatello, M. *Macromolecules* **1995**, *28*, 1887.
(9) Busico, V.; Cipullo, R.; Talarico, G.; Segre, A. L.; Chadwick, J. C. *Macromolecules* **1997**, *30*, 4786.
(10) Randall, J. C. *Macromolecules* **1997**, *30*, 803.
(11) Paukkeri, R.; Vaananen, T.; Lehtinen, A. *Polymer* **1993**, *34*, 2488.
(12) Paukkeri, R.; Lehtinen, A. *Polymer* **1994**, *35*, 1673.
(13) Lehtinen, A.; Paukkeri, R. *Macromol. Chem. Phys.* **1994**, *195*, 1539.
(14) Morini, G.; Albizzati, E.; Balbontin, G.; Mingizzi, I.; Sacchi, M. C.; Forlini, F.; Tritto, I. *Macromolecules* **1996**, *29*, 5770.
(15) Cheng, S. Z. D.; Janimak, J. J.; Zhang, A.; Hsieh, E. T. *Polymer* **1991**, *32*, 648.
(16) Janimak, J. J.; Cheng, S. Z. D.; Giusti, P. A.; Hsieh, E. T. *Macromolecules* **1991**, *24*, 2253.
(17) Janimak, J. J.; Cheng, S. Z. D.; Zhang, A.; Hsieh, E. T. *Polymer* **1992**, *33*, 728.
(18) Monasse, B.; Haudin, J. M. *Colloid Polym. Sci.* **1985**, *263*, 822.
(19) Alamo, R. G.; Chi, C. Crystallization Behavior and Properties of Polyolefins. In *Molecular Interactions and Time-Space Organization in Macromoleculer Systems*; Morishima, Y., Norisuye, T., Tashiro, K., Eds.; Springer: Berlin, 1999; p 29.
(20) Alamo, R. G.; Galante, M. J.; Mandelkern, L.; Lehtinen, A.; Paukkeri, R. *J. Therm. Anal.* **1996**, *47*, 913.
(21) Alamo, R.; Kim, M.-H; Galante, M. J.; Isasi, J. R.; Mandelkern, L. *Macromolecules* **1999**, *32*, 4050.
(22) Viville, P.; Daoust, D.; Jonas, A. M.; Nysten., B.; Legras, R.; Dupire, M.; Michel, J.; Debras, G. *Polymer* **2001**, *42*, 1953.
(23) Xu, J.; Feng, L.; Yang, S.; Yang, Y.; Kong, X. *Eur. Polym. J.* **1998**, *34*, 431.
(24) Busico, V.; Cipullo, R.; Corradini, P.; De Biasio, R. *Macromol. Chem. Phys.* **1995**, *196*, 491.
(25) Busico, V.; Cipullo, R.; Monaco, G.; Talarico, G.; Vacatello, M.; Chadwick, J. C.; Segre, A. L.; Sudmeijer, O. *Macromolecules* **1999**, *32*, 4173.
(26) Chadwick, J. C.; Miedema, A.; Ruiseh, B. J.; Sudmeijer, O. *Makromol. Chem.* **1992** *193*, 1463.
(27) De Rosa, C.; Auriemma, F.; Circelli, T.; Waymouth, R. M. *Macromolecules* **2002**, *35*, 3622.
(28) Chûjô, R. *Kagaku* **1981**, *36*, 420.
(29) Doi, Y. *Makromol. Chem., Rapid Commun.* **1982**, *3*, 635.
(30) Hayashi, T.; Inoue, Y.; Chûjô, R.; Asakura, T. *Polymer* **1988**, *29*, 138.
(31) Randall, R. C.; Alamo, R. G.; Agarwal, P. K.; Ruff, C. J. Macromolecules **2003**, *36*, 1572.
(32) Kaminsky, W.; Hähnsen, H.; Külper, K.; Woldt, R. US Patent 4,542,199, 1985.
(33) Watkins, J. J.; Krukonis, V. J.; Condo, P. D., Jr.; Pradhan, D.; Ehrlich, P. *J. Supercrit. Fluids* **1991**, *4*, 24−31.
(34) Britto, L. J. D.; Soares, J. B. P.; Peulidis, A.; Krokonis, V. *J. Polym. Sci., Polym. Phys. Ed.* **1999** *37*, 553.
(35) Gassi, A.; Zambelli, A.; Resconi, L.; Albizzati, E.; Mazzocchi, R. *Macromolecules* **1988**, *21*, 617.
(36) Busico, V.; Cipullo, R.; Monaco, G.; Vacatello, M.; Segre, A. L. *Macromolecules* **1997**, *30*, 6251.
(37) Soga, K.; Shiono, T. *Makromol. Chem., Rapid Commun.* **1987**, *8*, 305.
(38) Busico, V.; Cipullo, R.; Monaco, G.; Vacatello, M.; Bella, J.; Segre, A. L. *Macromolecules* **1998**, *31*, 8713.
(39) This definition of the rate of crystallization ($1/t_{0.5} = d(X_c)/dt$) assumes constant volume during the transformation and a constant final degree of crystallinity, X_c, at any crystallization temperature.
(40) VanderHart, D. L.; Alamo, R. G.; Nyden, M. R.; Kim, M. H.; Mandelkern, L. *Macromolecules* **2000**, *22*, 6078.
(41) Nyden, M. R.; VanderHart, D. L.; Alamo, R. G. *J. Comput. Theor. Polym. Sci.* **2002**, *11*, 175.
(42) The last fraction, obtained at the highest pressure was not available for ^{13}CNMR analysis.

(43) Alamo, R. G.; Blanco, J. A.; Agarwal, P. Manuscript in preparation.
(44) Hoffman, J. D.; Frolen, L. J.; Ross, G. S.; Lauritzen, J. I. *J. Res. Natl. Bus. Standars* **1975**, *79A*, 671.
(45) Ergoz, E.; Fatou, J. G.; Mandelkern, L. *Macromolecules* **1972**, *5*, 147.
(46) Fatou, J. G.; Marco, C.; Mandelkern, L. *Polymer* **1990**, *31*, 1685.
(47) Magill, J. H.; Li, H. M. *Polymer* **1978**, *19*, 416.
(48) Hoffman, J. D. *Polymer* **1982**, *23*, 656.
(49) Lopez, L. C.; Wilkes, G. L. *Polymer* **1988**, *29*, 106.
(50) Alamo, R. G.; Fatou, J. G.; Guzman, J. *Polymer* **1982**, *23*, 379.
(51) Alamo, R. G.; Mandelkern, L. *Macromolecules* **1991**, *24*, 6480.
(52) Chen, H.-L.; Li, L.-J.; Ou-Yang, W.-C.; Hwang, J. C.; Wong, W.-Y. *Macromolecules* **1997**, *30*, 1718.
(53) Brückner, S.; Meille, S. U.; Petraccone, U.; Pirozzi, B. *Prog. Polym. Sci.* **1991**, *16*, 361.
(54) Lotz, B.; Graff, S.; Straupe, S.; Wittmann, J. C. *Polymer* **1991**, *32*, 2902.
(55) Fatou, J. G. *Encyclopedia of Polymer Science and Engineering*, 2nd ed.; John Wiley & Sons: New York, 1989; Suppl. Vol., p 231.
(56) Allen, R. C.; Mandelkern, L. *Polym. Bull. (Berlin)***1987**, *17*, 473.
(57) Alamo, R.; Fatou, J. G.; Guzman, J. *Polymer* **1982**, *23*, 374.
(58) Wagner, J.; Phillips, P. J. *Polymer* **2001**, *42*, 8999.
(59) Ziabicki, A.; Alfonso, G. C. *Colloid Polym. Sci.* **1995**, *273*, 317.
(60) Kaminsky, W. *Metal Organic Catalyst for Synthesis and Polymerization*; Springer: Berlin, 1999; p 601.

MA021549G